Cellulose
DOI 10.10071s10570-013-0019-z

ORIGINAL PAPER

Influence of drying method on the material properties of nanocellulose I: thermostability and crystallinity

Yucheng Peng · Douglas J. Gardner · Yousoo Han · Alper Kiziltas · Zhiyong Cai · Mandla A. Tshabalala

Received: 1 February 2013/Accepted 4 August 2013

Abstract The effect of drying method on selected material properties of nanocellulose was investigated. Samples of nanofibrillated cellulose (NFC) and cellulose nanocrystals (CNC) were each subjected to four separate drying methods: air-drying, freeze-drying, spray-drying, and supercritical-drying. The thermal stability and crystallinity of the dried nanocellulose were evaluated using thermogravimetric analysis (TGA) and X-ray diffraction. Supercritical-drying produced NFCs with the least thermal stability and the lowest crystallinity index. Air-drying or spray-drying produced NFCs which were more thermally stable compared with freeze-dried NFCs. The CNCs dried by the three methods (air-drying, freeze-drying, and spray-drying) have similar onset temperature of thermal degradation. The different drying methods resulted in various char weight percentages at 600 °C for the dried NFCs or CNCs from TGA measurements. The dried NFCs are pure cellulose I while the dried CNCs consist of cellulose I and II. The calculated crystallinity indices differ with each drying method. The cellulose II content in CNCs changes as a function of drying method. For the application of nanocellulose in non polar thermoplastics, spray-dried products are recommended according to their higher thermal stability and higher crystallinity index.

Keywords Nanofibrillated cellulose · Cellulose nanocrystal · Thermostability Crystallinity

Y. Peng · D. J. Gardner (✉) · Y. Han · A. Kiziltas
Advanced Structures and Composites Center, University of Maine, 35 Flagstaff Road, Orono, ME 04469, USA
e-mail: douglasg@maine.edu

Y. Peng · D. J. Gardner · Y. Han · A. Kiziltas
School of Forest Resources, University of Maine, 35 Flagstaff Road, Orono, ME 04469, USA

A. Kiziltas
Department of Forest Industry Engineering, Faculty of Forestry, University of Bartin, 74100 Bartin, Turkey

Z. Cai · M. A. Tshabalala
Forest Products Laboratory, USDA Forest Service, One Gifford Pinchot Drive, Madison, WI 53726-2398, USA

Introduction

Nanocellulose, as a new generation of nano-scale material from forest products, has received considerable attention (Wegner and Jones 2006; Eichhorn et al. 2010; Habibi et al. 2010; Siqueira et al. 2010; Moon et al. 2011; Klemm et al. 2011). Cellulose is the primary structural building block of trees and other plants, and can be economically extracted from the wood fibers–an abundant and renewable resource. Regardless of its source, cellulose can be characterized as a high molecular weight linear homopolymer composed of D-anhydroglucopyranose units (AGU) which are linked

Published online: 11 August 2013

together by ß-(1 → 4)-glycosidic bonds (Klemm et al. 1998). In woody plants, these cellulose linear chains aggregate to highly ordered structures referred to as nanofibrils or elementary fibrils. These nanofibrils of cellulose are then packed into larger units to form microfibrils which in turn are assembled into cellulose fibers such as the pulp fibers. Nanofibrils in the woody plant are nano-scale fibers with average cross-sectional dimensions of about 10 nm × 3.5 nm. They consist of crystalline and amorphous domains with cellulose chains parallel to the nanofibril axis (Fengel and Wegener 1998; Chakraborty et al. 2005; Gardner et al. 2008). The nanofibrils are generally produced from the wood fiber, plant fiber, pulp fiber, microcrystalline cellulose (MCC), and microfibrillated cellulose (MFC) using mechanical or chemical methods (Moon et al. 2011). Processing dilute slurries of cellulose fibers, including wood fiber, plant fiber, and pulp fiber, by grinding or high-pressure homogenizing action produces nanofibrillated cellulose (NFC) (Herrick et al. 1983; Moon et al. 2011), while digestion of amorphous cellulosic domains of the raw materials through an acid hydrolysis process produces cellulose nanocrystals (CNC) (Hubbe et al. 2008). During the mechanical fibrillation process, the treatment of the raw materials with oxidation mediated by 2, 2, 6, 6-tetramethylpiperidine-1-oxyl (TEMPO) radical facilitates the disintegration of the materials into individual nanofibrils (Saito et al. 2006). NFC can also be utilized as a raw material for producing CNC. These nanocellulose suspensions including CNC and NFC suspensions are produced on the pilot scale and are commercially available in US and Canada (Bloch 2011; Ferguson 2012; Wallace 2012).

Each AGU of a cellulose chain possesses three hydroxyl groups at C-2, C-3, and C-6 positions, which can form hydrogen bonds. An extended network of hydrogen bonds consisting of inter- and intra-molecular bonds is responsible for the aggregation of cellulose chains which form the crystalline and amorphous regions. The high mechanical properties of cellulose fibers are also attributed to the formation of complicated hydrogen bonding networks among cellulose chains. The Young's modulus of the crystalline domain has values that range from 115 to 140 GPa (Sakurada et al. 1962; Matsuo et al. 1990; Nishino et al. 1995; Ishikawa et al. 1997). Young's modulus, measured in the direction perpendicular to the chain axis, was recently reported to be 14.8 ± 0.8 GPa, and in the chain axis direction it was reported to be 220 ± 50 GPa (Diddens et al. 2008). Compared with stainless steel, the strength-to-weight ratio of cellulose nanocrystals (CNCs) is said to be eight times higher (Ferguson 2012; Cranston et al. 2012). Because of their relatively high mechanical properties, nanocellulose has great potential as reinforcement in new bio composites, innovative bio plastics, and advanced reinforced composite materials. Because nanocellulose fibrils are produced as aqueous slurries that cannot be used as such in the manufacture of plastic composites, new drying techniques of the nanocellulose suspensions are required. A highly desirable feature of a good drying method is preservation of the morphology of the nanocellulose and its properties. In a previous study, four drying methods were investigated (Peng et al. 2012a). The study showed that three methods [freeze-drying (FD), supercritical-drying (SCD), and spray-drying (SD)] produced nano-scale cellulose fibrils.

From the point view of producing a dry form of nanocellulose for developing natural fiber reinforced thermoplastics, two material properties must be considered thermal stability and crystallinity. In the extrusion of plastic composites reinforced with lignocellulosic fibers, the compounding temperature of the composite is commonly restricted to about 200 °C because lignocellulosic materials start to degrade at approximately 230 °C. Cellulose, the most thermally stable constituent in the lignocellulosic materials, has a glass transition temperature in the range of 200–230°C and thermal decomposition starts at about 260 °C (Goring 1963; Gardner et al. 2008). The thermal stability of nanocellulose, compared with traditional cellulose fibers may be influenced by various factors, including processing conditions and their high surface to volume ratio. Indeed, one study showed that the thermal stability of dried nanofibrillated cellulose (NFC) decreased as a result of homogenization and drying processes (Quievy et al. 2010). For CNCs obtained by chemical hydrolysis using sulfuric acid, the presence of sulfate groups on the cellulose surface decreased their thermal stability (Roman and Winter 2004). Freeze and air-drying were also observed to have some influence on the thermal stability of CNC (Rämänen et al. 2012).

A high modulus of elasticity is expected from highly crystalline cellulose material. The Young's modulus of cellulose material depends on its crystallinity and the interaction of amorphous and crystalline regions (Cabrera et al. 2011). The arrangement of crystalline

and amorphous regions of cellulose fiber is proposed as "longitudinally arranged molecules change from one ordered region to the subsequent one, the transition areas being less ordered regions" (Fengel and Wegener 1998; Chakraborty et al. 2005). In the study of Cabrera et al. (2011), the Young's modulus of crystalline part was measured as 200–355 GPa while the bulk modulus of cellulose was measured as 20 GPa, indicating the superior mechanical properties of the crystalline region compared to the amorphous region. As a result, the higher crystallinity of nanocellulose may result in potentially higher mechanical properties in reinforced composites according to the rule of mixtures. On the other hand, the water holding capacity of nanocellulose is related to its crystallinity. When nanocellulose fibrils are included in composites, the absorption of water by cellulose fibrils severely degrades the properties of the composites (Espert et al. 2004). According to Nakamura et al. (1981), the amount of freezing bound water decreases with increasing degree of crystallinity in cellulose fibers. The effect of various drying methods on the crystallinity of dissolving-grade sulphite pulp was studied by Kouris et al. (1958). The drying methods included air drying, oven drying, freeze drying and freeze drying with a series of solvent exchanges in the cellulose pulp. The results indicated that no change in the crystallinity index occurred except a lower value was obtained from freeze drying cellulose fibers in benzene.

The present study focuses on the effect of different drying methods on the crystallinity and thermal properties of CNCs and NFCs. Samples of NFC and CNC suspensions were dried by freeze-drying, supercritical-drying, or spray-drying. The thermal properties of dried products were characterized by thermogravimetric analysis (TGA). The crystalline structure of nanocellulose was investigated by X-ray diffraction (XRD). Air-dried suspensions were used as controls. The effect of different drying methods on the thermostability and crystalline structures of NFCs and CNCs is discussed.

Experimental

Suspension preparation and drying

The NFC suspension was a commercial product, ARBOCEL MF40-10 at 10 wt% from J. Rettenmaier & Sohne GMBH + CO.KG, Germany. The CNC suspension at 6.5 wt% was obtained from the Forest Products Laboratory in Madison, Wisconsin. Before drying, distilled water was added into the original suspensions and mixed using a Speed Mixer® (Flack Tek Inc., US) for 4 min at 2,000 rpm to obtain final weight concentration of CNC and NFC suspensions at 2 wt%.

Different drying methods were applied to the nanocellulose suspensions at 2 wt%, including NFC and CNC suspensions, just after mixing. Air-drying (AD) of the two different suspensions was performed in a conditioning room with relative humidity of 65 ± 5 % and temperature of 20 ± 2 °C. The suspensions were allowedto settle to a constant weight in plastic containers before collection. Prior to freeze-drying (FD), CNF suspensions (about 20 ml) were frozen in vials at a temperature of −80ºC for 24 h. Frozen suspensions were then transferred to a Virtis Freezemobile 25 SL freeze dryer, which has a condenser temperature of −80 °C and a vacuum of 11 mTorr. Lyophilization was allowedto continue for 72 h. Supercritical drying (SCD) of the prepared suspension was conducted on the Tousimis Samdri PVT-3 Critical-Point dryer. Four steps were involved in this process: (1) dehydration of CNF suspension with a series of ethanol solutions (50, 75, 95, and 100 %) until water was completely replaced with ethanol (2) replacement of ethanol with liquid CO_2, (3) pressurization and heating of the liquid CO_2 and the cellulose mixture to the supercritical conditions, and (4) slow decompression of the supercritical CO_2 to atmospheric pressure. Spray-drying of the CNF suspensions was conducted using a Buchi Mini Spray Dryer B-290 laboratory spray dryer (New Castle, DE, USA). High purity nitrogen gas was used as an injected gas to form the suspension droplets. The spray-drying process is detailed in Peng et al. (2012a and b). In this study, nanocellulose suspensions were dried at an inlet temperature of 175 °C, gas flow rate of 540 1/h, pump rate of 4.5 ml/min, and drying gas flow rate of approximately 35 m^3/h. The outlet temperatures of the spray-dryer measured for the NFCs and CNCs were 89 and 92 °C, respectively. All the dried NFCs and CNCs were put in plastic bags and stored in a desiccator at ambient temperature to prevent moisture absorption.

Thermogravimetric analysis (TGA)

Thermal properties of dried nanocellulose and a commercial product of microcrystalline cellulose

(MCC) with the brand name of Emcocel® SP15 from Rettenmaier and Sohne GMBH + CO.KG (Germany), which was used a control, were characterized using a Mettler Toledo System consisting of the STARe Software and the TGA/SDTA851e module. All tests were performed in a nitrogen atmosphere with a ceramic sample pan. Analysis of individual nanocellulose samples weighing 1–2 mg was carried out at a constant heating rate of 10 °C/min between 25 to 600 °C. Each sample was tested in triplicate. The TGA thermal curve was displayed as weight percent (%) versus temperature. After the TGA test, the residual nanocellulose fibrils were examined by scanning electron microscopy.

Scanning electron microscopy (SEM)

The morphologies of the air-dried samples were studied by SEM using an AMR 1000 (AMRay Co.) scanning electron microscope. All samples were sputter-coated with gold before the microscopic observations were obtained. SEM images were taken at an accelerating voltage of 10 kV at various magnifications. The samples of dried nanocellulose after TGA testing were directly studied by SEM using the Hitachi Tabletop Microscope SEM TM 3000 (Hitachi High-Technologies Corporation, Tokyo, Japan) at an accelerating voltage of 15 kV.

X-ray diffraction (XRD) characterization

XRD analyses of dried nanocellulose were performed on a high resolution X-ray diffractometer (Model X'Pert PRO, Philips PANalytical, Netherlands) with nickel-filtered copper Kα (0.154 nm) radiation generated at 45 kV and 40 mA. The dried nanocellulose materials were pressed manually into cylindrical wafers with a diameter of 2 cm and thickness of 0.05−0.1cm using a Dake Press (Drake, Grand Falls, MI). A silicon zero background plate was used to calibrate the effect of sample holder and to make sure no signal was generated from the sample holder. The same sample holder position and sample holder (holder and silicon zero background plate) were used for all experiments. Scans were obtained from 5° to 40'' 20 in 0.02 degree steps for 2.5 s per step. Subtraction of background intensity from the measured intensity of nanocellulose samples was performed first and then normalization of the maximum peak intensity of nanocellulose materials to an intensity of 10,000 was conducted. Crystallinity index (CI) of dried nanocellulose samples was calculated using the empirical method described by Segal et al. (1959). The equation is shown in the following:

$$CI = 100 \times \frac{I_{200} - I_{am}}{}$$

where I_{200} is the maximum intensity of the principal peak (200) lattice diffraction (at 22.7° of 2θ for cellulose I, and 21.7° of 20 for cellulose II), and I_{am} is the intensity of diffraction attributed to amorphous cellulose (at 18° of 20 for cellulose I, and at 16° of 20 for cellulose II) (Segal et al. 1959; Azubuike et al. 2012; French and Sntiago Cintrón 2013). This method is convenient and quick to determine the relative crystallinity of nanocellulose which can be used for relative comparisons. A comparison of CI of the nanocellulose including NFCs and CNCs caused by different drying methods was conducted. The effect of different drying methods on the crystallinity of nanocellulose was also evaluated using the methods of Gjønnea and Norman (1958, 1960).

Results and discussion

Thermal properties of dried nanocellulose

Thermal properties of cellulosic materials have been intensively studied (Shafizadeh 1984; Maschio et al. 1992; Li et al. 2001; Shen and Gu 2009; Peng et al. 2011). Cellulose as one of the main components, its thermal decomposition is principally responsible for the production of flammable volatiles, which are released through dehydration, hydrolysis, oxidation, decarboxylation and transglycosylation (Levan 1989). The pathway of thermal decomposition and the composition of the cellulose fibers (residual hemicelluloses) are influenced by many physical and chemical factors such as temperature, type of atmosphere, size and texture of the cellulose sample, crystallinity, presence of impurities such as metals, and other parameters (Shafizadeh 1984). The thermal behavior of dried nanocellulose, including NFC and CNC, was characterized by thermogravimetric analysis (TGA) in nitrogen.

Representative TGA curves of dried NFC and CNC at a heating rate of 10 °C/min are shown in Figs. 1a and 2a. The results of the three tests for each sample

were consistent. Based on the weight percentage change as a function of temperature, each TGA curve can be divided into three regions. For example, region I of the TGA curve of the MCC control sample is defined as the initial mass loss portion found from 25 °C to about 216 °C. In region I, the slight mass loss is below 3.1 ± 0.1 % (The standard deviation is calculated based on the three measurements) and is mainly caused by the evaporation of water from the cellulosic samples. No thermal degradation occurred in this region. The detailed TGA curve of the MCC sample in region I is shown in Figs. 1b and 2b. For the MCC sample in region I, the mass loss increased to about 3.1 % at 110 °C and continued at a plateau until about 216 °C (Fig. 1b). Region II for the MCC sample in the TGA curve (Fig. 1a) is defined as the major mass loss stage, starting at the temperature where the mass loss deviated from the plateau region (about 216 °C in Fig. 1b). The temperature of 216 °C (the ending temperature of region I shown in Table 1) is defined as the onset temperature of thermal degradation for the MCC sample. In region II, two different degradation mechanisms were proposed by Kilzer and Broido (1965): (1) dehydration of cellulose by an endothermic process to produce "dehydrocellulose" between about 200 and 280 °C and (2) depolymerization of cellulose in competition with dehydration between 280 and 340 °C, resulting in the formation of volatiles. Decomposition of dehydrocellulose formed in the first path into gases and char residue becomes dominant at about 320 °C. Evolution of CO_2, H_2O and CO with formation of solid char is mainly observed. If depolymerization occurs more extensively than dehydration, volatilization of tar (high boiling products, HPB) mostly composed of levoglucosan is observed. The HBP might further decompose, with the production of light flammable gases, if it is not promptly removed from the heating zone. The mass residue and temperature at the end of region II are 12.5 ± 0.3 wt% and 358 °C as shown in Table 1. After region II, the mass loss rate of the cellulosic samples decreased (Fig. 1a). The TGA curve starting from this point to the final testing temperature of 600 °C is defined as region III. For the MCC sample, region III starts at a temperature of 358 °C. In region III at a temperature above 500 °C, the levoglucosan breaks down to provide a variety of low molecular weight fission products, including hydrocarbons and hydrogen as well as CO, CO_2 and H_2O. Secondary reactions may occur in the gas phase as further decomposition of

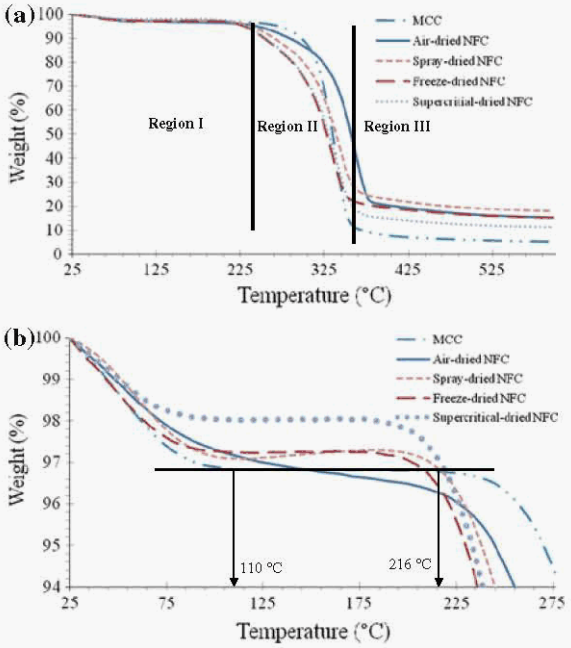

Fig. 1 TGA curves of dried NFC and MCC at a heating rate of 10 °C/min **a** from 25 to 600 °C and **b** from 25 to 276 °C in detail

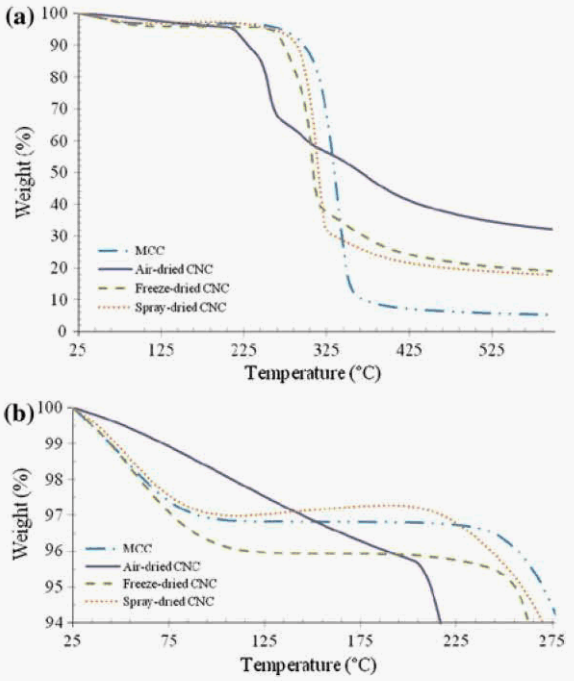

Fig. 2 TGA curves of dried CNC and MCC at a heating rate of 10 °C/min **a** from 25 to 600 °C and **b** from 25 to 276 °C in detail

levoglucosan, in the solid phase as the condensation and crosslinking of intermediate chars to highly condensed polycyclic aromatic structures, or by interaction of both phases as gasification of char by reaction with H_2O and CO_2 at high temperatures to produce CO and H_2 (Shafizadeh 1982). At a temperature of 600 °C, the final char residue for the MCC sample is 5.4 ± 0.3 wt% (Table 1).

The dried NFCs showed similar thermal behaviors compared to the MCC sample (Fig. la). A close-up examination of region I in Fig. lb indicated that the dried NFCs showed almost the same TGA curve trend as the MCC sample. The elimination of residual water from the NFC samples occurs first with increasing temperature and then a plateau of constant mass of the dried NFC is reached as all the residual moisture evaporates. A similar mass loss rate was observed at the beginning of region I for all the samples (Fig. lb) indicating that the water content within the dried NFC samples was the same for the samples dried by the different methods. The evaporation rate appears to be consistent. Depending on the amount of the residual water in the dried NFCs, the plateau temperatures are not the same. Supercritical-dried NFCs reach the plateau temperature first with the least mass loss of 1.9 ± 0.1 %, indicating that supercritical-drying produced NFCs with about 1.9 % moisture content (Table 1). Freeze-dried (3.1 ± 0.6) and spray-dried (2.8 ± 0.1) NFCs have a similar moisture content while the commercial MCC sample has a moisture content of 3.1 %. The residual moisture contents for all the dried samples are summarized in Table 1. The TGA curve of air-dried NFCs differed slightly from all the others in this stage (region I). The evaporation of water from air-dried NFCs can be further divided into two phases. In phase I, the mass loss rate of air-dried NFCs is the same as all the other cellulosic samples. In phase II, the mass loss rate is less than that in phase I (Fig. lb). No constant mass loss plateau was observed for air-dried NFCs in region I. Air-drying of the NFC suspension formed a bulk material with a solid packing of nanofibrils (Fig. 4a, b). During the TGA test, the surface moisture of the NFC bulk material evaporated first, resulting in same mass loss rate as with all the other cellulose samples. As the temperature increased at 10 °C/min, the solidly packed surface phase limits residual moisture diffusion from inside of the bulk material to the surface, resulting in a decreased rate of mass loss in Fig. lb. At the same time, the final mass loss of 4.1 ± 0.5 % in region I shown in Fig. lb indicated that the air-dried NFCs possessed higher moisture content when compared with NFCs dried by the other methods. As the temperature continues to increase, the NFCs undergo thermal decomposition. This onset temperature of thermal degradation is critical for the applications of NFCs in reinforcing thermoplastics. Different drying methods provide different onset temperature of thermal degradation. The degradation temperatures for all the dried NFCs are shown in Table 1. The MCC is the most thermally stable cellulose samples in this study, followed by air-dried and spray-dried NFCs. The least

Table 1 Thermal stability and crystallinity of dried nanocellulose

Sample	Drying method	Crystallinity index (%)	Region I		Region II		Region III
			Temperature (°C)	Moisture residue (wt%)[a]	Temperature (°C)	Mass residue (wt%)[a]	Mass residue (wt%)[a]
MCC	–	–	216	3.1 ± 0.1	358	12.5 ± 0.3	5.4 ± 0.3
NFC	AD	74.9	207	4.1 ± 0.5	375	23.3 ± 1.6	15.9 ± 0.8
	FD	80.7	186	3.1 ± 0.6	350	24.8 ± 0.8	15.4 ± 0.3
	SD	82.1	204	2.8 ± 0.1	367	26.1 ± 0	18.1 ± 0.1
	SCD	73.3	184	1.9 ± 0.1	370	16.7 ± 0.2	11.5 ± 0.1
CNC	AD	–	205	4.6 ± 0.2	–	–	31.9 ± 0.5
	FD	–	205	3.9 ± 0.4	317	37.3 ± 1.2	18.5 ± 0.7
	SD	–	206	2.6 ± 0.5	330	30.5 ± 0.1	18.4 ± 0.5

AD air-drying, *FD* freeze-drymg, *SD* spray-drying, *SCD* supercritical-drying

[a] Standard deviation is calculated based on the three measurement of thermogravimetric analysis

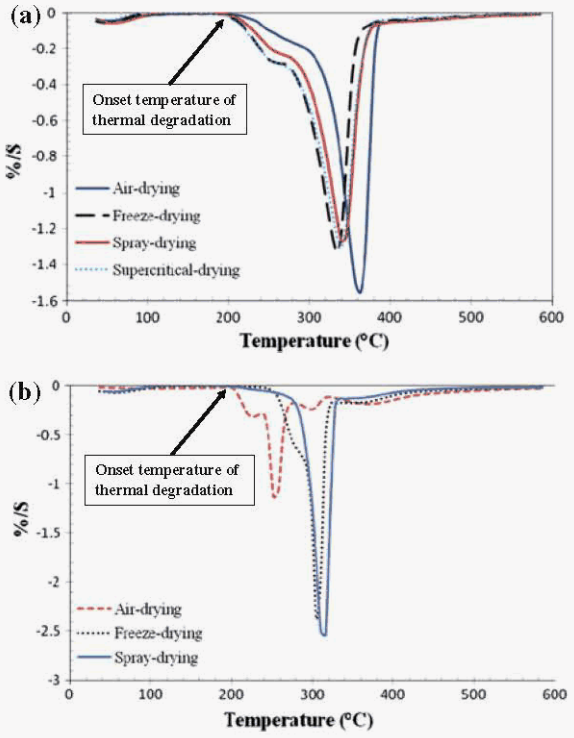

Fig. 3 DTG curves of the dried NFCs (**a**) and CNCs (**b**)

thermally stable sample is supercritical-dried and freeze-dried NFCs. During the thermal degradation processes in the regions II and III, cellulose samples dried by different methods showed different results. The ending temperatures of region II are different for the NFCs dried by different methods (Table 1). Air-dried NFCs end region II at the highest temperature of 375 °C among all the dried NFCs and the ending temperature for the spray-dried NFCs is 367 °C. Under the same temperature of region II, the mass residue of air-dried NFCs is higher than that of spray-dried NFCs, followed by freeze-dried and supercritical-dried NFCs. The TGA curve of freeze-dried NFCs in region II almost completely overlaps with those of supercritical-dried samples (Fig. la). However, they performed differently in region III and freeze-dried NFCs enter the region III at a lower temperature (350 °C) than those of supercritical-dried materials (370 °C) (Table 1). The mass residue of freeze-dried NFC in region III is much higher than that of supercritical-dried materials. The final char residue of freeze-dried NFCs at 600 °C is about 15.4 ± 0.3 % while the value for supercritical-dried NFCs is about 11.5 ± 0.1 %. The behavior of the air-dried NFCs was the same as the freeze-dried NFCs in region III except the different starting temperatures (Table 1). Spray-dried NFCs have the highest char residue among all the samples in region III and the final char residue at 600 "C is about 18.1 ± 0.1 %. Air-drying NFC suspensions formed solidly packed material (Fig. 4a, b) while the other three drying methods formed nanostructured materials (Peng et al. 2012a, b). Compared with air-dried material, the other three drying methods provide higher surface area for the same weight of the cellulose material, resulting in the greater mass loss rates in region II of thermal decomposition via the TGA tests. At the same time, supercritical-drying produced finely divided, smaller diameter nanocellulose fibrils while freeze-drying and spray-drying produced larger sized nanocellulose fibrils (Peng et al. 2012a). As a result, the final mass residue of supercritical-dried NFCs is the lowest. For spray-dried NFCs, agglomerated fibrils or irregular shaped materials were formed (Peng et al. 2012a, b). During the process of water evaporation at relatively high temperature, the surface nanofibrils become closely packed, forming a solid shell layer. The thermal degradation of the spray-dried NFCs started on the surface first and then a compact charcoal protection layer formed to reduce thermal degradation of the inner fibrils. This behavior is validated by the micrograph shown in Fig. 4a. The spray-dried NFC single fibrils and agglomerates retain their original shape during the TGA test up to 600 °C. Finally, the highest char residue was observed for the spray-dried NFCs. During air-drying, the long drying time precipitated the larger sized NFC fragments at the bottom of the drying container. After drying, a solid packed top surface and porous structured bottom surface were formed (Fig. 4c, d). For spray-dried NFCs as shown in Fig. 4e, agglomerated fibrous and spherical NFCs were produced (Peng et al. 2012b). As a result, the packing of nanofibrils for air-dried NFCs is not as tight as the nanofibrils produced by spray-drying NFCs, indicating the lower final mass residue of the air-dried NFCs. For freeze-drying, the nanofibrils were first confined in the space between ice crystals during the freezing process (Svagan et al. 2008; Sehaqui et al. 2010), increasing the concentration of nanofibrils locally. At this point, the interaction among nanocellulose fibrils is enhanced and the nanofibrils form a similar agglomerate structure as occurring in the case of the air-drying process. This would explain the

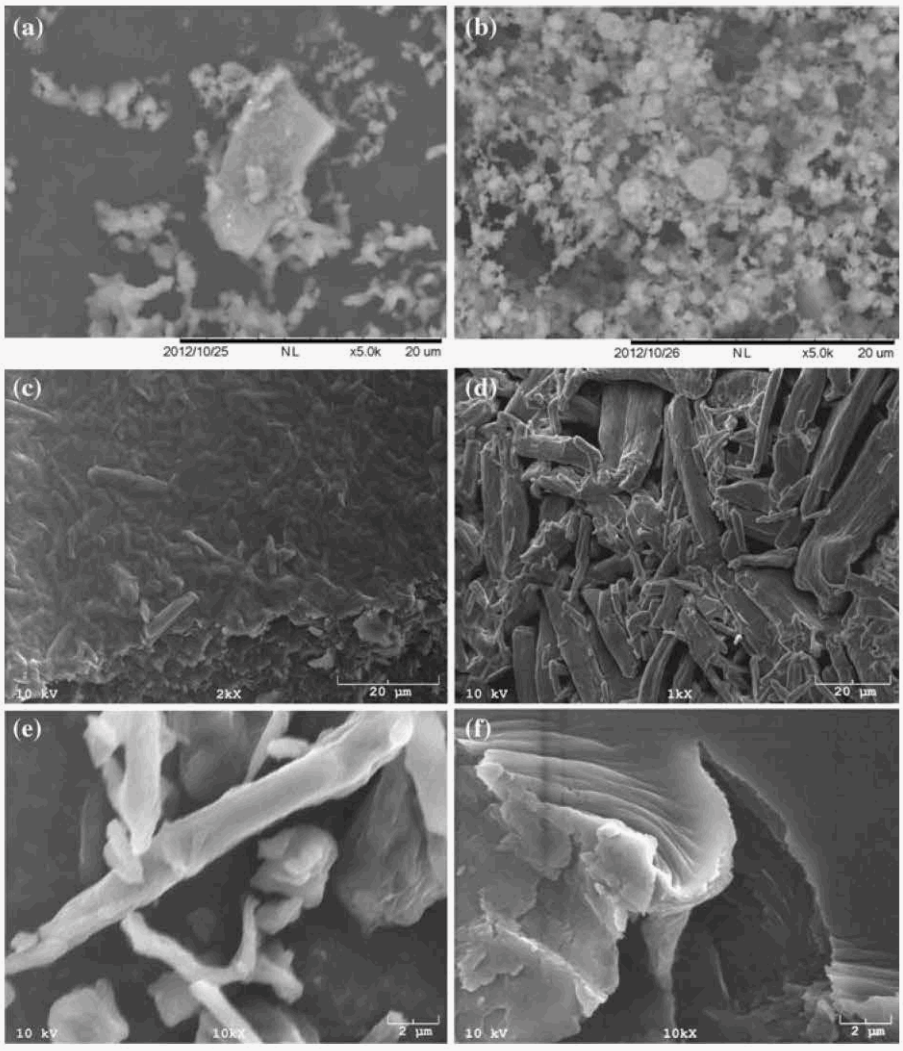

Fig. 4 SEM mcrographs **a** TGA test residues of spray-dried NFCs, **b** TGA test residues of spray-dried CNCs, **c,** air-dried NFC top surface, **d** air dried NFC bottom surface, **e** spray dried NFC, and **f** air dried CNC

identical thermal behaviors and similar char residues of the freeze-dried and air-dried NFCs in region III (Fig. la; Table 1).

The first derivative curves of the TGA (DTG) scans for the dried NFCs are shown in Fig. 3a. DTG curves represent the mass loss rate of the materials at different temperatures. For the dried NFCs, two peaks are observed in the DTG curves. The first small peak represents the mass loss caused by the residual moisture evaporation which is identified in region I of the TGA curves. The second peak is a continuous phase and mainly represents the major mass loss stage. This peak starts from the onset temperature of thermal degradation until the final testing temperature of 600 °C. The onset temperatures for the second peak are different among the NFCs dried by different methods, which were previously discussed for the TGA scans. At the same temperature, the different values observed in the DTG curves in the second peak phase indicate that the NFC samples dried by various drying methods have different mass loss rates. From the vertex point of the second DTG peak, the temperature of the greatest mass loss rate can be extracted. From Fig. 3a, the temperatures of the greatest mass loss rate for the dried NFCs are identified as: 363 °C for air-dried sample, 340 °C for spray-dried and supercritical-dried samples, and 328 °C for freeze-dried sample.

Supercritical-drying of CNC suspension was not possible in this study (Peng et al. 2012a). The thermal behaviors of the CNC dried by other methods are similar with those of NFCs and the TGA curves are shown in Fig. 2a and b. Simultaneously, the DTG curves are shown in Fig. 3b. The CNCs were less thermally stable than the MCC sample. Analysis of the thermal behaviors of dried CNC in region I showed that (1) spray-dried CNC has similar moisture content (2.6 ± 0.5 %) with those of spray-dried NFCs (2.8 ± 0.1 %); (2) Freeze-dried CNC has slightly higher moisture content (3.9 ± 0.4 %) than both freeze-dried NFCs (3.1 ± 0.6 %) and spray-dried CNC (2.6 ± 0.5 %). The water evaporation region can also be identified in the DTG curves shown in Fig. 3b. At the same time, the thermal behavior of air-dried CNC differs from all the other cellulose samples under the testing conditions. For the freeze-dried and spray-dried CNC samples, a plateau of mass residue occurred before the onset temperature of thermal degradation. For air-dried CNC material, the initial mass loss increased linearly with increasing temperature until the onset temperature of thermal degradation (205 °C). The CNC mass loss rate of the air-dried sample is also less than those of freeze-dried and spray-dried samples. The low mass loss rate can be demonstrated by the DTG curves shown in Fig. 3b. The low mass loss rate indicates that the evaporation of water from air-dried CNC is more difficult than the CNCs dried by the other two methods. Air-drying of CNC suspension formed a tightly packed material with a very smooth surface (Fig. 4f). The surface layer functioned as a dense thermoplastic, slowing down the evaporation of water from inside of the bulk material. The onset temperatures of thermal degradation of the dried CNC samples were determined and these data are shown in Table 1. The effect of drying methods on the onset temperatures of thermal degradation of CNCs is not obvious and the dried CNCs are slightly more thermally stable than those of NFC samples. From the DTG curves in Fig. 3b, it can also be seen that the dried CNCs started to degrade at similar temperatures, i.e. similar onset temperature of thermal degradation. However, the mass loss rate after the onset temperature of thermal degradation is completely different (Fig. 3b). Air-dried CNCs have the highest mass loss rate followed by the spray-dried sample. The freeze-dried sample has the lowest mass loss rate following the onset temperature of thermal degradation among the three samples. From the DTG curves shown in Fig. 3a, it can be seen that the behaviors of mass loss rate of the air-dried CNCs differ significantly from the CNCs dried by the other two methods. In the significant thermal degradation phases (regions II and III in the TGA curves), only one peak is observed in the DTG curves of freeze-dried and spray-dried CNC samples while multiple peaks are identified in the DTG curves of air-dried CNCs (Fig. 3b). The temperature of the greatest mass loss rate for the air-dried CNCs is 253 °C which is much lower than those of freeze-dried CNCs (305 °C) and spray-dried CNCs (311 °C). The char residues at the end of region II for freeze-dried and spray-dried CNCs are 37.3 ± 1.2 and 30.5 ± 0.1 wt% as shown in Table 1. Division of the TGA curve of air-dried CNCs into regions II and III is vague and the char residue in region II is not shown in Table 1. The higher final mass residues of the dried CNCs forced the temperature spans of region II for the dried CNC into a narrower band than those of the dried NFCs. The final char residues of the air-dried and freeze-dried CNC samples are 31.9 ± 0.5 and 18.5 ± 0.7 wt% which are higher than those of corresponding NFC samples (15.9 ± 0.8 and 15.4 ± 0.3 wt% for air-dried and freeze-dried samples) (Fig. 2a; Table 1). The manufacturing process of CNC may partially contribute to the observed behavior. The addition of sulfuric acid into the cellulose increased the carbon yield at high temperature (Kim et al. 2001). For spray-dried CNCs, the final char residue (18.4 ± 0.5 %) at 600 °C is similar with that of the spray-dried NFCs (18.1 ± 0.1 %). Spray-drying of CNC suspensions formed spherical or donut shaped materials with hard shells (Peng et al. 2012b). The solid shell formed may prevent the thermal degradation of the inside CNCs and exhibit a similar thermal degradation mechanism with the spray-dried NFCs. The SEM micrograph of the final CNC residues after the TGA test is shown in Fig. 4b. Almost intact spherical shapes of the thermally degraded CNCs are observed. Therefore, spray-drying produced NFC and CNC having similar final char residues. However, the final char residues are significantly different for air-dried NFCs and CNCs (Table 1). Air-dried CNC char residue is 31.8 ± 0.5 wt% while air-dried NFC char residue is 15.9 ± 0.8 wt%. In addition, air-dried CNCs have significantly higher char residue than the freeze-dried and spray-dried CNC samples. This result is consistent

with the observation of Rämänen et al. (2012). The TGA curve of air-dried CNCs in region II and III obviously differs from the others (Fig. 2a). During air-drying of the CNC suspension, the slow water evaporation rate allows the CNCs to rearrange in a preferred order. A hydrogen bonded network is created among the cellulose nanocrystals when the sample is dried to a constant weight. The hydrogen bonded network assembled for air-dried CNCs is also different from that for air-dried NFCs because of the different structures and the much smaller size of the CNCs. During the TGA test, thermal decomposition of the air-dried CNCs occurred in three phases: (1) the CNC sample first started to lose residual water; (2) the hydrogen bonding network assembled among the CNCs during drying started to thermally degrade; and (3) the thermal decomposition of CNCs themselves occurred. The thermal behaviors as defined by these three steps differ from the other NFCs and slow down the thermal decomposition of air-dried CNC. Therefore, a relatively high char residue weight percentage was observed.

X-ray diffraction (XRD) characterization

The X-ray diffraction spectra of dried nanocellulose are shown in Fig. 5a, b. The peaks shown in the X-ray diffraction pattern are the composite peaks combining several different crystalline planes (Guinier 1963; French and Sntiago Cintrón 2013). The major diffraction peaks at 2θ = 14.8°, 16.3°, 22.6° and 34.5'' in Fig. 5a were assigned as the crystalline planes with Miller indices of -110, 110, 200 and 004 in the crystal structure of cellulose I (Langan et al. 2001; Nishiyama et al. 2002). However, the intensity for each peak is not the real diffraction intensity of the assigned single crystalline plane. These peaks are the composite peaks of diffraction intensity of the assigned crystalline plane with several other crystalline planes (Langan et al. 2001; Nishiyama et al. 2002, 2003; French and Sntiago Cintrón 2013). The assigned crystalline plane contributes the major portion of the intensity shown in the Fig. 5a. For example, the peak at 2θ = 14.8 observed in Fig. 5a is a combination of diffraction signals from crystalline planes of 011, 101, and −110 with the dominant signal of the crystalline plane of −110 (Nishiyama et al. 2002, 2003; French and Sntiago Cintrón 2013). Overlapping of the diffraction signals of these crystalline planes broadened the width

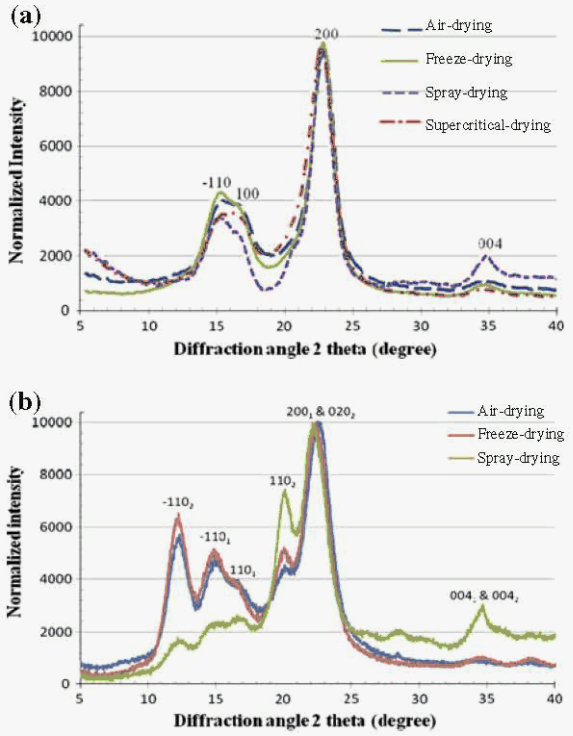

Fig. 5 X-ray diffraction spectra of dried nanocellulose: **a** NFC and **b** CNC. Subscript 1 and 2 represent cellulose I and II

of the obtained diffraction peaks. Diffraction spectra of dried CNCs differ from those of NFCs. According to the assignment of X-ray diffraction peaks to cellulose crystalline planes, dried CNCs include two polymorphs: cellulose I and II (Garvey et al. 2005; Qi et al. 2009; Langan et al. 2001; Nishiyama et al. 2002, 2003; French and Sntiago Cintrón 2013). Peaks in Fig. 5b at 2θ = 12.1° and 19.8° are assigned to crystalline planes with Miller indices of −110 and 110 for cellulose II (Langan et al. 2001; French and Sntiago Cintrón 2013). Peaks at 2θ = 14.9° and 16.4° are mainly caused by the diffraction of the crystalline planes of −110 and 110 from cellulose I (Nishiyama et al. 2002; French and Sntiago Cintrón 2013). Simultaneously, the peak intensities at 2θ = 12.1°, 19.8°, 14.9° and 16.4° does not represent the diffraction signal of the single crystalline planes of −110, 110 from cellulose II and −110,110 from cellulose I, respectively. These peaks are also composite peaks overlapped with the diffraction signal from other crystalline planes. It is worth noting that crystalline planes of 200 (at 2θ = 22.6°) and 004 (at 2θ = 34.5°) were observed in both celluloses I and II at the same

position of the diffraction spectra as shown in Fig. 5a and b. The diffraction signals of crystalline planes of 200 from cellulose I, 020 from cellulose II, and 004 from cellulose I and II in CNCs contributed to the observed diffraction peaks shown in Fig. 5b. Different manufacturing processes result in the different crystalline composition of NFC and CNC. During the manufacturing of CNC, cellulose II was generated in the suspension because of the sulfuric acid treatment (Krassig 1993) while mechanically nanofibrillated cellulose did not change the cellulose polymorphs.

Quantitative characterization of the portions of the crystalline region in the dried nanocellulose was also conducted. The crystallinity indices of the dried NFCs corrected for the background signal measured without cellulose samples were calculated directly from the height ratio between the intensity of the crystalline peak ($I_{200} - I_{am}$) and total intensity (I_{200}) (Segal et al. 1959). In this method, the characterized sample is assumed to consist of two components: crystalline and amorphous regions. The amount of the crystalline region is represented by the intensity of the highest diffraction peak and the amount of amorphous region is represented by the minimum intensity between the major peaks (French and Sntiago Cintrón 2013). However, the highest diffraction peak and the minimum intensity are a composite signal combined with the signals from the other crystalline planes. The method of Segal et al. (1959) cannot resolve the absolute value of the crystallinity index of the material. According to the calculations of Nishiyama et al. (2002 and 2003) and French and Sntiago Cintrón (2013), overlapping at the highest diffraction peak of cellulose I (crystalline plane of 200 at $2\theta = 22.6°$) is not significantly affected by the signal from the other crystalline planes. At the same time, the impact of the diffraction signal from crystalline plane of 111 located at 2θ between 18° and 20° on the minimum intensity between the major peaks is not significant in cellulose I (Nishiyama et al. 2002, 2003; French and Sntiago Cintrón 2013). Therefore, the Segal crystallinity index provides reliable relative crystallinity of the dried nanocellulose for comparison purposes. The calculated values of crystallinity indices are shown in Table 1. Spray-dried products showed the highest crystallinity index of 82.1 % compared with the other drying methods. This high crystallinity index can be partially explained by the heat treatment of the NFCs during the spray-drying process. The highest temperature the NFCs experienced during the spray-drying process was 89 °C (Peng et al. 2012b). Heat treatment can increase the crystallinity of cellulose (Bhuiyan et al. 2000; Yildiz and Gümüşkaya 2007). At the same time, recrystallization of amorphous cellulose was also observed with heat and humidity (Hermans and Weidinger 1946; Wadehra et al. 1965; Kimura et al. 1974; Hatakeyama 1981). The spray-drying process provides these heat and humidity conditions. The agglomeration of nanocellulose fibrils may provide another opportunity to increase the crystallinity index of spray-dried NFCs. Under non-aqueous conditions or highly concentrated solutions of cellulose, hydrogen bonding can occur directly among the hydroxyl groups of the cellulose chains (Tanaka and Fukui 2004). The hydrogen-bonding drives nanocellulose fibrils to approach each other closely and form tight aggregates resulting in the formation of crystalline structures. Supercritical-drying produced single NFC entangled with a crystallinity index of 73.3 %. The crystalline regions did not change during the drying process. For air-drying and freeze-drying, the nanocellulose fibrils rearrange, forming samples with higher crystallinity indices of 74.9 and 80.7 % compared with that of the supercritical-dried sample. With the normalization of the diffraction intensity of dried nanocellulose, comparison of the crystallinity index of the dried nanocellulose can be easily performed as shown in Fig. 5a. The minimum intensities between major peaks for the dried nanocellulose are in the order: supercritical-drying > air-drying > freeze-drying > spray-drying. For the dried CNC samples, calculation of crystallinity index is not as simple as the dried NFCs. It can be seen from Fig. 5b that, drying methods significantly affect the diffraction patterns of the dried nanocellulose. For the complicated diffraction pattern, the relative crystallinity index cannot be evaluated directly. The dried CNC samples consist of cellulose I and II. The superposition of the 002 plane makes it impossible to calculate the crystallinity index for the cellulose I component using the method of Segal et al. (1959). At the same time, the height and the shape of the peaks in the X-ray spectra are strongly influenced by the presence of the two polymorphs. However, the proportion of each component in the dried CNC samples can be approximately determined by the method of Gjønnes and Norman (1960). But this was not the goal of the present study. Examination of the

relative crystallinity changes resulting from different drying methods is the point. Based on the method of Gjønnes and Norman, the intensity ratio of 110 plane in cellulose II to 200 & 020 plane in the X-ray spectra ($I[11O_2]/I[200_1$ & $020_2]$) is linearly related to the component of cellulose I in the mixture (Gjønnea and Norman 1960). The intensity ratios ($I[110]/I[200_1$ & $020_2]$) measured in Fig. 5b are 0.47, 0.54, and 0.76 for air-dried, freeze-dried, and spray-dried CNCs, indicating that different drying methods produced different proportions of cellulose I and II in the mixture with the same starting CNC suspension. Simultaneously, the peak locations of the crystalline plane of 200, & 020_2 were observed to be linearly increased with increasing cellulose II content. The shifts of 200_1 & 020_2 peak location to lower Bragg angles further demonstrated that the proportions of cellulose II in the mixture decreased in the order: air-dried > freeze-dried > spray-dried. The higher cellulose II content may partially explain the thermal behavior of the dried CNC samples. Cellulose II crystals have better thermal stability than that of cellulose I (Yue 2011). The higher content of cellulose II results in higher final char residues for the dried CNC samples (Fig. 2a).

Conclusions

The effects of drying methods on the thermostability and crystallinity of nanocellulose, including nanofibrillated cellulose and cellulose nanocrystals, were investigated. Four drying methods were employed air-drying, freeze-drying, spray-drying, and supercritical-drying. Each drying method produced unique nanocellulose fibril sizes and morphologies. Supercritical-drying generated NFCs with the least thermal stability and the lowest crystallinity index. Air-drying and spray-drying formed NFCs and CNCs with similar onset temperatures of thermal degradation. Freeze-dried CNCs are more thermally stable than the freeze-dried NFCs. Different drying methods also resulted in different char residue weight percentages at 600 °C for the same starting materials of NFC or CNC. The dried NFCs are pure cellulose I while the dried CNCs consist of cellulose I and II. The calculated crystallinity indices differ with each drying method. The cellulose II content in CNCs is a function of each drying method. On the basis of their relatively superior thermal stability and higher crystallinity index, it is reasonable to expect sprayed-dried nanocellulose to be more suitable for the application in non polar thermoplastics compared with air-dried or freeze-dried, or supercritical-dried nanocellulose.

Acknowledgments We acknowledge the financial support from Maine Economic Improvement Fund and the USDA Forest Service Forest Product Laboratory The content and information does not necessarily reflect the position of the funding agencies. Much appreciation goes to J. Rettenmaier & Söhne GMBH Company for donating the nanofibrillated cellulose.

References

Azubuike CP, Rodríguez H, Okhamafe AO, Rogers R D (2012) Physicochemical properties of maize cob cellulose powders reconstituted from ionic liquid solution. Cellulose 19(2):425-433

Bhuiyan MTR, Hirai N, Sobue N (2000) Changes of crystallinity in wood cellulose by heat treatment under dried and moist conditions. J Wood Sci 46:431-436

Bloch J(2011) UMaine to build nation's only cellulose nanofibrils pilot plant. http://umaine.edu/news/blog/2011/10/28/umaine-to-build-nation's-only-cellulose-nanofibrils-pilot-plant/

Cabrera RO, Meersman F, McMillan PF, Dmitriev V (2011) Nanomechanical and structural properties of native cellulose under compressive stress. Biomacromolecules 12: 2178–2183

Chakraborty A, Sain M, Kortschot M (2005) Cellulose microfibres as reinforcing agents for structural materials. In: Oksman K, Sain M (eds) Cellulose nanocomposites: processing, characterization and properties. American Chemical Society, Washington, DC, pp 169–186

Cranston ED, Kan KHM, Eita M, Johansson E, Netrval J, Salajkova M, Arwin H, Wågberg L (2012) Mechanical testing of thin film nanocellulose materials. http://www.tappi.org/Hide/Events/2012-Nanotechnology-Conference/Papers/12NANO05.aspx. Accessed 28 Sept 2012

Diddens I, Murphy B, Krisch M, Muller M (2008) Anisotropic elastic properties of cellulose measured using inelastic X-ray scattering. Macromolecules 41:9755–9759

Eichhorn SJ, Dufresne A, Aranguren M, Marcovich NE, Capadona JR, Rowan SJ, Weder C, Thielemans W, Roman M, Renneckar S, Gindl W, Veigel S, Keckes J, Yano H, Abe K, Nogi M, Nakagaito AN, Mangalam A, Simonsen J, Benight AS, Bismarck A, Berglund LA, Peijs T (2010) Review: current international research into cellulose nanofibres and nanocomposites. J Mater Sci 45:l–33

Espert A, Vilaplana F, Karlsson S (2004) Comparison of water absorption in natural cellulosic fibres from wood and one-year crops in polypropylene composites and its influence on their mechanical properties. Compos Part A Appl Sci Manuf 35(11):1267–1276

Fengel D, Wegener G (1998) Wood chemistry, ultrastructure, reactions. De Gruyter, Berlin

Ferguson W (2012) Why wood pulp is world's new wonder material. New Sci 2878:24

French AD, Sntiago Cintrón M (2013) Cellulose polymorphy, crystallite sire, and the Segal crystallinity index. Cellulose 20:583–588

Gardner DJ, Oporto GS, Mills R Samir MASA (2008) Adhesion and surface issues in cellulose and nanocellulose. J Adhes Sci Technol 22:545–567

Garvey CJ, Parker IH, Simon GP (2005) On the interpretation of X-ray diffraction powder patterns in terms of the nanostructure of cellulose I fibers. Macromol Chem Phys 206(15):1568–1575

Gjønnea J, Norman N (1958) The use of half width and position of the lines in the X-ray diffractograms of native cellulose to characterize the structural properties of the samples. Acta Chem Scand 12(10):2028–2033

Gjønnea J, Norman N (1960) X-ray investigations on cellulose II and mixtures of cellulose I and II. 1. A method for characterizing and determining the relative contents of the two modifications. Acta Chem Scand 14(3):683–688

Goring DAI (1963) Thermal softening of lignin, hemicelluloses and cellulose. Pulp Paper Mag Can 64(12):T517–T527

Guinier A (1963) X-ray diffraction in crystals, imperfect crystals, and amorphous bodies. W. H. Freeman and Company, San Francisco, London

Habibi Y, Lucia LA, Rojas OJ (2010) Cellulose nanocrystals: chemistry, self-assembly, and applications. Chem Rev 1103479–3500

Hatakeyama H (1981) Structural change of amorphous cellulose by water- and heat-treatment. Makromol Chem 182: 1655–1668

Hermans PH, Weidinger A (1946) On the recrystallization of amorphous cellulose. J Am Chem Soc 68(12):2547–2552

Herrick FW, Casebier RL, Hamilton JK, Sandberg KR (1983) Microfibrillated cellulose: morphology and accessibility. J Appl Polym Sci Symp 37:797–813

Hubbe MA, Rojas OJ, Lucia LA, Sain M (2008) Cellulosic nanocomposites: a review. BioResources 3(3):929–980

Ishikawa A, Okano T, Sugiyama J (1997) Fine structure and tensile properties of ramie fibers in the crystalline form of cellulose I, II, III_I and IV_I. Polymer 38:463-468

Kilzer FJ, Broido A (1965) Speculations on the nature of cellulose pyrolysis. Pyrodynamics 2:151–163

Kim D, Nishiyama Y, Wada M, Kuga S (2001) High-yield carbonization of cellulose by sulfuric acid impregnation. Cellulose 8:29–33

Kimura M, Hatakeyama T, Nakano J (1974) DSC study on recrystallization of amorphous cellulose with water. J Appl Polym Sci 18:3069–3076

Klemm D, Philipp B, Heinze T, Heinze U, Wagenknecht W (1998) Comprehensive cellulose chemistry. Fundamentals and analytical methods, Vol 1. Weinheim, New York, Chichester, Brisbane, Singapore, Toronto: Wiley-VCH VerlagGmbH, Weinheim 1

Klemm D, Kramer F, Moritz S, Lindstrom T, Ankerfors M, Gray D, Dorris A (2011) Nanocelluloses: a new family of nature-based materials. Angew Chem Int Ed Engl 50:5438–5466

Kouris M, Ruck H, Mason SG (1958) The effect of water removal on the crystallinity of cellulose. Can J Chem 36:931–948

Krässig HA (1993) Cellulose: structure, accessibility and reactivity. Gordon and Breach Science Publishers, Amsterdam, the Netherlands

Langan P, Nishiyama Y, Chanzy H (2001) X-ray structure of mercerized cellulose II at 1 A resolution. Biomacromolecules 2(2):410-416

Levan SL (1989) Thermal degradation. In: Schniewing AP (ed) Concise encyclopedia of wood & wood-based materials, 1st edn. Pergamon Press, Elmsford, NY, pp 271–273

Li S, Lyons-hart J, Banyasz J, Shafer K (2001) Real-time evolved gas analysis by FTIR method an experimental study of cellulose pyrolysis. Fuel 80:1809–1817

Maschio G, Koufopanos C, Lucchesi A (1992) Pyrolysis, a promising route for biomass utilization. Bioresour Technol 42219–231

Matsuo M, Sawatari C, Iwai Y, Ozaki F (1990) Effect of orientation distribution and crystallinity on the measurement by X-ray diffraction of the crystal lattice moduli of cellulose I and II. Macromolecules 23:3266–3275

Moon RJ, Marini A, Nairn J, Simonsen J, Youngblood J(2011) Cellulose nanomaterials review: structure, properties and nanocomposites. Chem Soc Rev 40:3941–3994

Nakamura K, Hatakeyma T, Hatakeyma H (1981) Studies on bound water of cellulose by differential scanning calorimetry. J Text Inst 72(9):607–613

Nishino T, Takano K, Nakamae K (1995) Elastic modulus of the crystalline regions of cellulose polymorphs. J Polym Sci Polym Phys 33:1647–1651

Nishiyama Y, Langan P, Chanzy H (2002) Crystal structure and hydrogen-bonding system in cellulose Iß from synchrotron X-ray and neutron fiber diffraction. J Am Chem Soc 124(31):9074–9082

Nishiyama Y, Sugiyama J, Chanzy H, Langan P (2003) Crystal Structure and hydrogen bonding system in cellulose Iα from synchrotron X-ray and neutron fiber diffraction. J Am Chem Soc 125:14300-14306

Peng Y, Shi SQ, Ingram L (2011) Chemical emissions from adhesive-bonded wood products at elevated temperatures. Wood Sci Technol 45:627–644

Peng Y, Gardner DJ, Han Y (2012a) Drying cellulose nanofibrils: in search of a suitable method. Cellulose 19(1): 91–102

Peng Y, Han Y, Gardner DJ (2012b) Spray-drying cellulose nanofibrils: effect of drying process parameters on particle morphology and sire distribution. Wood Fiber Sci 44(4): 448-461

Qi H, Cai J, Zhang L, Kuga S (2009) Properties of films com-Dosed of cellulose nanowhiskers and a cellulose matrix regenerated from alkali/urea solution. Biomacromolecules 10(6):1597–1602

Quievy N, Jacquet N, Sclavons M, Deroanne C, Paquot M, Devaux J (2010) Influence of homogenization and drying on the thermal stability of microfibrillated cellulose. Polym Degrad Stab 95:306–314

Rämänen P, Penttilä PA, Svedström K, Maunu SL, Serimaa R (2012) The effect of drying method on the properties and nanoscale structure of cellulose whiskers. Cellulose 19(3):901–912

Roman M, Winter WT (2004) Effect of sulfate groups from sulfuric acid hydrolysis on the thermal degradation behavior of bacterial cellulose. Biomacromolecules 5:1671–1677

Saito T, Nishiyama Y, Putaux J, Vignon M, Isogai A (2006) Homogeneous suspensions of individualized microfibrils

from TEMPO-catalyzed oxidation of native cellulose. Biomacromolecules 7(6):1687–1691

Sakurada I, Nukushina Y, Itoh T (1962) Experimental determination of the elastic modulus of crystalline regions in oriented polymers. J Polym Sci 57:651–660

Segal L, Creely JJ, Martin AE Jr., Conrad CM (1959) An empirical method for estimating the degree of crystallinity of native cellulose using the X-ray diffractometer. Text Res J 29(10):786-794

Sehaqui H, Salajkova M, Zhou Q, Berglund LA (2010) Mechanical performance tailoring of tough ultra-high porosity foams prepared from cellulose I nanofiber suspensions. Soft Matter 6:1824–1832

Shafizadeh F (1982) Introduction to pyrolysis of biomass. J Anal Appl Pyrolysis 3:283–305

Shafizadeh F (1984) The chemistry of pyrolysis and combustion. In: Rowell RM (ed) The chemistry of solid wood. the American Chemical Society, Seattle, Washington, pp 489–529

Shen DK, Gu S (2009) The mechanism for thermal decomposition of cellulose and its main products. Bioresour Technol 100:6496–6504

Siqueira G, Bras J, Dufresne A (2010) Cellulosic bionanocomposites: a review of preparation, properties and applicatioins. Polymers 2:728–765

Svagan AJ, Azizi Samir MAS, Bergund LA (2008) Biomimetic foams of high mechanical performance based on nanostructured cell walls reinforced by native cellulose nanofibrils. Adv Mater 20:1263–1269

Tanaka F, Fukui N (2004) The behavior of cellulose molecules in aqueous environments. Cellulose 11:33–38

Wadehra IL, Manley R, St J (1965) Recrystallization of amorphous cellulose. J Appl Polym Sci 9:2627–2630

Wallace R (2012) USDA under Secretary Sherman unveils nanocellulose production facility. http://blogs.usda.gov/2012/08/03/usda-under-secretary-sherman-unveils-nanocellulose-production-facility/

Wegner TH Jones PE (2006) Advancing cellulose-based nanotechnology. Cellulose 13:115–118

Yildiz S, Gümüşkaya E (2007) The effects of thermal modification on crystalline structure of cellulose in soft and hardwood. Build Environ 42:62-67

Yue Y (2011) A comparative study of cellulose I and II fibers and nanocrystals. School of renewable natural resources (Vol. Master of Science). Louisiana State University, Baton Rouge